Supplementary Information of the Manuscript:

On the choice of optimal reservoir operating rules in a changing climate for the sustainable management of drinking water sources

Mattia Neri [a], *Elena Toth* [a]

[a] Department of Civil, Chemical, Environmental and Materials Engineering, University of Bologna, Italy

Correspondence to: mattia.neri5@unibo.it

Journal: ***Water Resources Management***

S1 Reservoir System and Demand Data

Data and information regarding the reservoir management history and constraints
Operators and managers of the utility company provided reservoir geometrical and hydraulic relationships (including information about current reservoir management rules, operative constraints on intakes, releases, outlet flows, environmental flows and their changes over time, and maximum allowed annual withdrawals). They also supported the experiment by detailing the safety, flood control and maintenance protocols, historical evolution over time of the adopted management rules and information about past water saving measures during drought conditions. Hourly time series (starting from 1996) of historical reservoir level and inflow from the tunnel pipe, as well as daily time series of withdrawal volumes and release flows from the bottom outlets were also made available, along with hourly river streamflow measures in correspondence of the intakes on the nearby rivers connected through the tunnel.

Historical water demand from the supply network and information about the other Local Sources
Monthly historical consumption data starting from year 2009 are available for each of the almost 200 delivery points across the water distribution network. Delivery points are classified based on the water source that supplies them (i.e. the Ridracoli reservoir or which of the Local Sources), therefore allowing to analyze the different contributions across the years. Along with consumption time series, information about technical constraints and allowed withdrawal volumes for each Local Source were also provided by the water supply company.

S2 GCM-RCM modelling chains

Table S1 Ensemble of GCM-RCM modelling chains used for simulate future climate forcings.

Institute	RCM	Driving GCM
CLMcom	CCLM4-8-17	CNRM-CERFACS-CNRM-CM5
		ICHEC-EC-EARTH
		MPI-M-MPI-ESM-LR
DMI	HIRHAM5	ICHEC-EC-EARTH
KNMI	RACMO22E	ICHEC-EC-EARTH
SMHI	RCA4	CNRM-CERFACS-CNRM-CM5
		ICHEC-EC-EARTH
		IPSL-IPSL-CM5A-MR
		MOHC-HadGEM2-ES
		MPI-M-MPI-ESM-LR

S3 TUW model description and parameterization

The TUW model is a version of the HBV model (Bergström, 1976; Lindström et al., 1997) developed by Viglione and Parajka (2018). It consists of a snow module, a soil moisture module and a flow response and routing module. The inputs are daily air temperature, precipitation and potential evapotranspiration over the different elevation zones. In this study, potential evapotranspiration is derived from temperature time series using the simplified method proposed by Blaney and Criddle (1962). The snow module is based on a simple degree-hour concept, and it is ruled by five parameters: two threshold temperature parameters distinguishing rain and snow, *Tr* and *Ts*, a melting temperature *Tm*, a snow correction factor *SCF* and the degree-hour factor *DDF*. The soil moisture module represents soil moisture state changes and runoff generation. It involves three parameters: the maximum soil moisture storage *FC*, a parameter representing the soil moisture state above which evapotranspiration is at its potential rate, *LP*, and a parameter β ruling the non-linear function of runoff generation. Finally, an upper and a lower soil reservoirs and a triangular transfer function compose the runoff response and routing module, involving seven additional parameters. The sum of excess rainfall and snowmelt enters the upper zone reservoir and leaves this reservoir through three paths: i) outflow from the reservoir based on a fast storage coefficient k_1; ii) percolation to the lower zone with a constant percolation rate C_{PERC}, iii) if a threshold of the upper storage state L_{UZ} is exceeded, through an additional outlet based on a very fast storage coefficient k_0. Water leaves the lower zone based on a slow storage coefficient k_2. The outflows from both reservoirs are then routed by a triangular transfer function representing runoff routing in the streams, where the base of the transfer function, B_Q, is estimated with the scaling of the outflow by the C_{ROUTE} and B_{MAX} parameters. More details about the model structure and application in R can be found in Parajka et al. (2007) and Ceola et al. (2015) respectively, while a graphical representation of the model scheme is reported by Neri et al. (2020).

A preliminary parameter sensitivity test (not showed here) allowed to set the parameter ranges. In particular, 10 out of the 15 total parameters are calibrated, while temperature parameters *Tr*, *Ts* and *Tm* are fixed respectively to 1.5, -1 and 0 °C, and *LP* is fixed to 0.7. Table S2 presents the parameters to be calibrated and the corresponding ranges.

Table S2. Calibrated TUW model parameters and their ranges

Parameter	Units	Range	Description
SCF	-	0.9 - 1.5	Snow correction factor
DDF	mm/(°C*day)	0 - 5	Degree day factor
FC	mm	0 - 600	Field capacity, i.e., max soil moisture storage
B	-	0 - 20	Non linear parameter for runoff production
k_0	days	0 - 2	Storage coefficient for very fast response
k_1	days	2 - 30	Storage coefficient for fast response
k_2	days	30 - 250	Storage coefficient for slow response
L_{UZ}	mm	1 - 100	Threshold storage state, very fast response starts if exceeded
C_{PERC}	mm/day	0 – 8	Constant percolation rate
B_{MAX}	days	0 - 10	maximum base at low flows
C_{ROUTE}	days ^{2}/mm	0 - 50	Scaling parameter

Calibration strategy: for each of the study catchments, the parameterisation of the model is performed by forcing it with E-OBS observed meteorological fields (Cornes et al., 2018) and minimising the differences between the simulated outputs and the observed records of daily discharges, available at the basin outlet during the period 1996-2021. For the basin closed at the dam, the time series of historical discharges is obtained thought the water balance at the reservoir considering the historical time series of the components of Eq. 1 in the Manuscript.
The sets of parameters of the rainfall-runoff model are estimated with an automatic model calibration procedure, using the Dynamically Dimensioned Search algorithm (DDS, Tolson and Shoemaker, 2007). The objective function to be maximised is the Kling-Gupta Efficiency (Gupta et al., 2009) between observed and simulated streamflow, defined as:

$$KGE = 1 - \sqrt{(r-1)^2 + (\alpha-1)^2 + (\beta-1)^2} \quad \text{(S1)}$$

where r is the Pearson product-moment correlation coefficient, α is the ratio between the standard deviations of the simulated and observed values and β is the ratio between the means of the simulated and observed values.
Usually, a standard model parameterisation would involve the use of a split-sample procedure, in which the available streamflow observation record is separated into two different sub-periods used respectively to train (i.e. calibrate parameters) and test (i.e. validate) the model. Here instead all the available observation records were entirely used for both model calibration and validation. In fact, since we know from preliminary tests that the models behave well in the study catchment, we preferred not to use a split-sample procedure and to have the longest possible time series of observed data for estimating model parameters.

Calibration performances: in addition to KGE, calibration performances are evaluated through Nash–Sutcliffe efficiency (Eq. 2) as well. While KGE considers different types of model errors (the error in the mean, the variability and the dynamics of runoff), NSE is a standardised version of the mean square error.

$$NSE = 1 - \frac{\sum(Q_{sim} - Q_{obs})^2}{\sum(Q_{obs} - \overline{Q_{obs}})^2} \quad \text{(S2)}$$

where Q_{sim} is the simulated runoff, Q_{obs} is the observed runoff and $\overline{Q_{obs}}$ is the average observed runoff. MSE-based metrics as NSE is traditionally used for the evaluation of performance regarding

high-flows, since they typically magnify simulation errors associated with the higher values of the distribution.
The model performances obtained by calibrating the two models, forced with observed meteorological fields, against the observed streamflow at catchment outlet during the calibration period (1996-2021) are satisfactory and the rainfall-runoff model behaves well in all the five basins: Kling–Gupta efficiencies ranges between 0.803 and 0.868, while Nash Sutcliffe efficiency ranges between 0.602 and 0.737.

S4 Assessment of the minimum demand from the reservoir

S4.1 Methodology

The minimum withdrawal volume represents such portion of demand which cannot be provided by the Local Sources at any given time *t*. Therefore, it depends both on the water demand from the customers served by the overall water supply network and on the capacity of the Local Sources themselves. This section reports the main steps of the methodology used for the assessment of minimum monthly demand flow from the Ridracoli reservoir mQ_j. The approach is based on three main steps.

Step 1: Subdivision of the water supply network into seven sub-networks
As described in the Manuscript, while the Ridracoli reservoir is serving the entire water distribution network, Local Sources provide water to limited portions of the region. Therefore, the regional water supply network can be divided into sub-networks based on the connection with the different Local Sources: seven sub-networks are identified, and the delivery points are grouped accordingly (see right panel in Figure S1).

Step 2: Analysis of the historical water consumption and definition of a critical demand scenario
For each sub-network S_k, the total historical water consumption $D_{k,j,y}$ during the *j*-th month of the year *y* is obtained by aggregating monthly water consumption data $D_{i,j,y}$ provided at each of the delivery points *i*:

$$D_{k,j,y} = \sum_{i \epsilon S_k} D_{i,j,y} \qquad k = 1, \dots, 7 \tag{S4}$$

Then, for each sub-network S_k, a monthly critical demand scenario $CD_{k,j}$ is defined by adopting for each month of the year *j*, the maximum consumption registered during the observation period in such month:

$$CD_{k,j} = \max_{y}(D_{k,j,y}) \qquad \begin{matrix} k = 1, \dots, 7 \\ j = 1, \dots, 12 \end{matrix} \tag{S5}$$

At the same time, the capacity (in terms of maximum monthly volumes) of the Local Sources serving each sub-network are assessed. In this case, such monthly potentially derivable volumes $PL_{k,j}$ are obtained based on regulatory and technical constraints.

Step 3: Computation of the minimum monthly volume necessarily needed from the Ridracoli reservoir
Finally, the minimum monthly demand volumes mD_j which must be provided to the users from the Ridracoli reservoir are calculated as the sum of the differences between the critical water demand scenarios and the capacity of the Local Sources obtained for each sub-network for any given month of the year *j*:

$$mD_j = \sum_{k=1}^{7} (CD_{k,j} - PL_{k,j}) \tag{S6}$$

Of course, the adopted approach assumes that the maximum monthly (critical) demand occurs simultaneously in all districts and throughout the entire reference period. While this assumption is highly conservative, considering the significant uncertainties regarding the future pattern of both potential of Local Sources and users' demand, which are assumed to be constant over time, a more cautious approach is preferred. On the other hand, we also assume that mD_j is equally distributed along the month j, therefore adopting a constant minimum monthly demand flow from the Ridracoli reservoir mQ_j:

$$mQ_j = \frac{mD_j}{86400 \cdot N_j} \tag{S7}$$

where N_j is the number of days in the j-th month of the year.

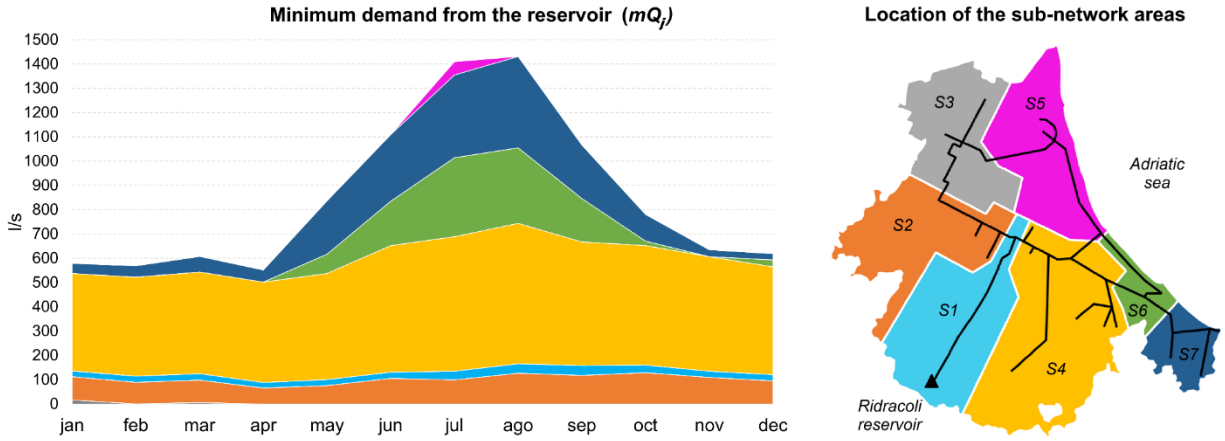

Figure S1 Minimum demand from the seven sub-networks (left) and corresponding rough Location of the seven sub-networks S_1, …, S_7 across the region and the entire water supply network (right).

S4.2 Results

Figure S1 shows the estimated minimum demand mQ_j, where the colored bands represent the contributions needed from the different sub-networks (left), along with the location of the corresponding sub-network supply areas (right). It is evident a strong seasonality in the demand, which confirms the need to define different monthly operating rules. Secondly, it is evident that the seasonal peaks are due to the demand in coastal, while the hinterlands (yellow, light blue and orange areas), that are less affected by summer tourism, are characterized by a nearly constant demand throughout the year (and the grey S3 area instead may rely, when needed, exclusively on its Local Sources).

The withdrawal volumes requested by coastal areas is consistently higher during spring and summer, especially in the Southern sub-networks S6 and S7. In fact, green and blue areas include the mass tourism destinations of Rimini and Riccione, along with a number of theme parks and related touristic services, which contributes substantially to the higher summer consumptions. On the other hand, the Northern coast (magenta, S5), where the summer demand is similarly high, is provided with more powerful Local Sources, in particular thanks to a new treatment plant of water retrieved from the Po river, and for such subnetwork there is only a small volume in July that must necessarily come from the reservoir.

S5 Formulation of withdrawal operating rules: graphical representation of the rule form

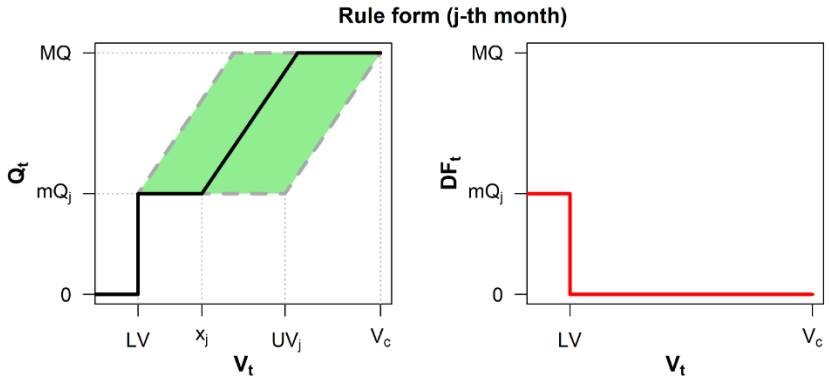

Figure S2 Graphical representation of the rule form. Left: the black line refers to the piecewise linear function which expresses the withdrawal Q_t as function of the stored volume V_t, while the green polygon represents the feasible rule domain. Right: the red line expresses the deficit volume DF_t as function of V_t.

S6 Performance of the GCM-RCMs in the historical control period

Figure S3 shows the validation of the selected climate modelling chains (Table S1) against observations (E-OBS) in order to verify their ability to adequately reproduce historical climate.
The left panel reports monthly mean areal precipitation (MAP) estimated for E-OBS and for the CORDEX raw and bias-corrected outputs over the five catchments feeding the reservoir in the reference control period 1981-2010. It shows the large variability of single raw climate model outputs (light shaded yellow lines), highlighting the need for the bias-correction. The adjusted (BC) series (light red lines) succeed in fact in re-aligning the seasonality to observations (blue line) and the ensemble mean of the BC scenarios (bold red line) closely approximates the reference precipitation (blue line). The discrepancy between the single adjusted BC chains and observed MAP is not negligible (up to around +/- 15 mm/months for some GCM-RCMs), but this outcome is overall satisfactory, considering that the bias-correction was performed at European scale (and not specifically over the study area) and based on a previous version of the E-OBS dataset used in this validation (for details, see Dosio, 2016).
The right panel illustrates the same results for the average daily minimum temperature (MATN). Similarly to what observed for mean areal precipitation, the bias-adjustment is needed to correct the bias of raw climate simulations. Similar results are obtained for maximum daily temperature (not showed here for brevity).

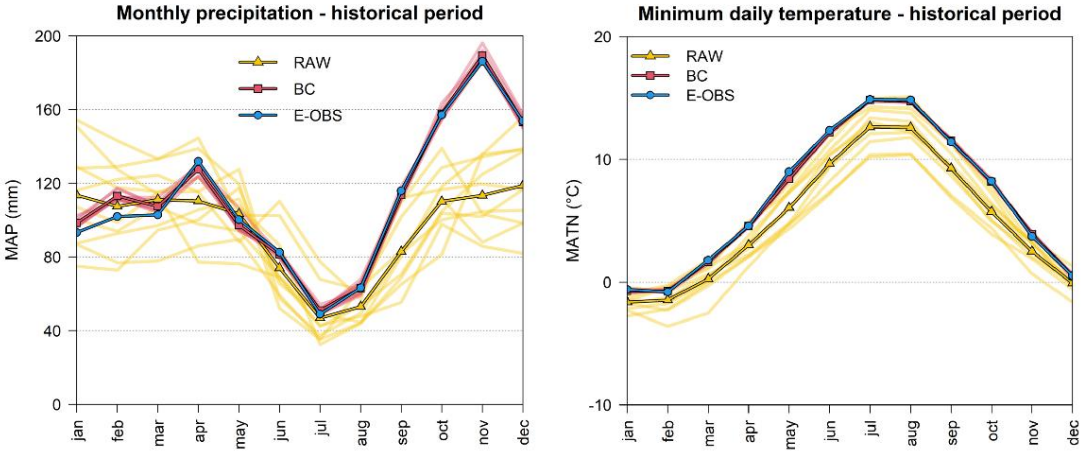

Figure S3 Comparison of GCM-RCM forcings over the catchments feeding the reservoir: monthly mean areal precipitation (MAP, left) and mean daily minimum temperature (MATN, right) in the reference control period. Blue line refers to observations (E-OBS), bolder yellow line to the RAW models ensemble mean, bolder red line to the BC model ensemble mean, light shaded lines to single climate models.

S7 Evaluation of simulation-optimization scenarios in the control period

To further verify the representativeness of the ensemble of GCM-RCM scenarios for simulating historical water availability and reservoir management, the outcomes of the simulation framework obtained in the historical period for OH and for the ten $CH_{1\text{-}10}$ optimization scenarios are compared. As explained in the main Manuscript, we remind that, in order to analyze and comparing the impact of the different rules on the two contrasting objectives and on the resulting reservoir behavior, two specific solutions for each Pareto front are here selected as possible reference among the possible optimal alternatives:

- the equal Trade-Off Solution (TOS), highlighted with bold dots in Figure 4, which is commonly used to evaluate optimization results and represents an equally balanced optimum solution.
- the Minimum Deficit Solution (MDS), which represents the solution corresponding to the lowest cumulated deficit volume during the entire simulation period , highlighted in Figure 4 with bold triangles.

Therefore, for the OH and for each of the ten $CH_{1\text{-}10}$ simulation-optimization scenarios, the modelling framework is simulated twice over the period 1982-2010 by adopting the operating withdrawal rules obtained respectively for the MDS and for the TOS solution of the corresponding front (for a total of 22 model runs). Figure S4 reports the long-term average of annual withdrawal (left panels), monthly withdrawal (central panels) and demand deficit volumes (right panels) respectively for the TOS (upper panels) and MDS (lower panels) Pareto solutions: blue bold line refers to OH scenario, shaded red lines to single $CH_{1\text{-}10}$ scenarios and the red bold line to their ensemble mean.

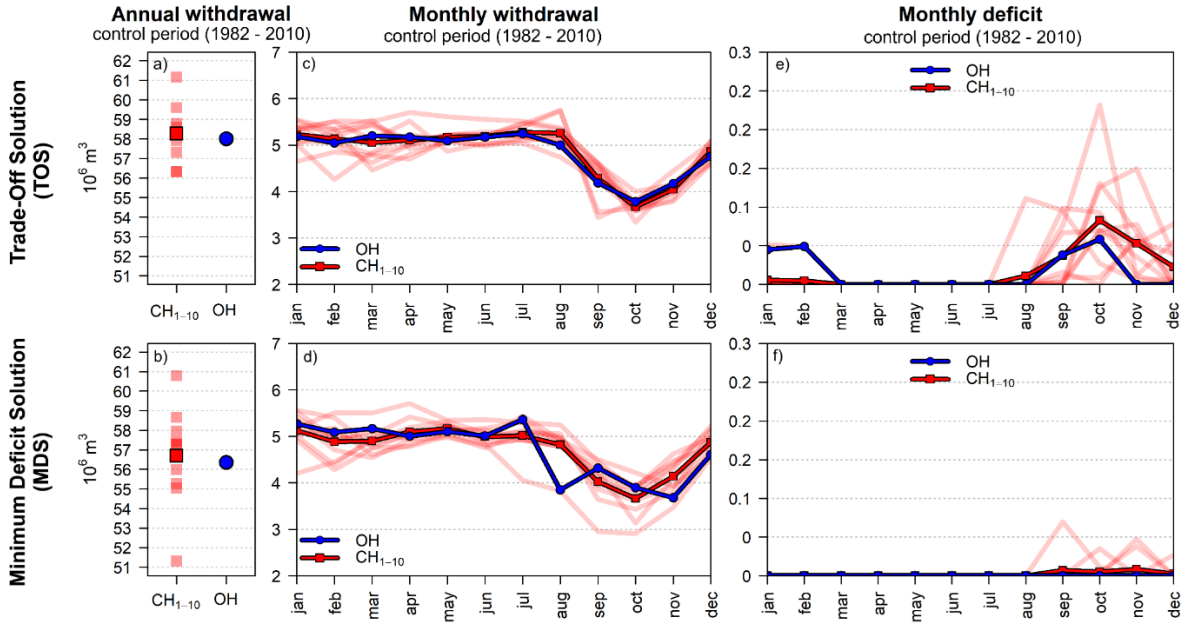

Figure S4 Long-term average annual withdrawal (left panels a and b), monthly withdrawal (central panels c and d) and average monthly deficit (right panels e and f) volumes simulated during the historical control period (1982-2010) by adopting the operating withdrawal rules of the TOS (top) and MDS (bottom) solutions of the observed-historical (blue) and CORDEX-historical (red, $CH_{1\text{-}10}$) optimizations. Shaded red lines refer to the individual GCM-RCM scenarios, bold red lines to the ensemble average.

Looking at the left panels, the ensemble averages of annual withdrawal volumes (bold red squares) of CORDEX scenarios are in line with the observed run (blue dots) corresponding to the same Pareto solution, and enables the visualization of the increase in withdrawal volumes, which settles at around 1.5 million m^3, achieved by using TOS operating rules instead of the minimum deficit ones. Both for TOS and MDS, the seasonality of withdrawal volumes (shown in the middle panels, panels c-d) is preserved between OH and $CH_{1\text{-}10}$ runs: supplied volumes are high and overall stable from January

to July, while they typically decrease at the end of the summer and in autumn, due to the high demand and low inflows that lead the reservoir to empty at the end of the touristic season. At the same time, when deficit volumes occur (panels e-f), they are concentrated between the end of the summer and the beginning of the winter, with the reservoir emptied by the summer uses and the autumn season precipitation sometimes late to arrive for filling it.

For the more conservative solution (MDS), it can be noticed in panel f that for the OH run and for some of the CH_{1-10} scenarios the deficit can be completely avoided, while for a few scenarios a zero-deficit solution is not found: this is expected since some of the GCM-RCMs slightly underestimate seasonal precipitation during the control period and, as we already argued, even small precipitation remaining bias could substantially affect the reservoir response to temporal dynamics of drought events, affecting the operating rules. For the same reason, the different CH_{1-10} scenarios result in more pronounced differences between the withdrawal volumes of MDS solutions (panel d) in respect to the spectrum obtained for the TOS rules (panel c): in fact the more priority is given to the minimization of deficits, the more sensitive is the system (and the operating rules) to singular occurrences of precipitation underestimates. When considering trade-off solutions (TOS) instead, a similar (relative) importance is given to the two objectives: operating rules are thus less dependent on single drought events and monthly withdrawal volumes exhibits less variability between different scenarios (panel c). On the other hand, such optimization does not focus on completely avoiding deficit conditions and since the deficit volumes strongly depends on the severity of the specific droughts, the pattern of average monthly demand deficit (light red lines in panel e) shows a large variability among the CH_{1-10} scenarios.

Despite the variability, the pattern of CORDEX-historical CH_{1-10} simulations overall agrees with that of the observed-historical OH run, especially when considering the ensemble average (bold red line). This confirms that the selected ensemble of GCM-RCMs may be considered suitable for simulating the historical (current) management of the system and can be used as reference to evaluate differences with simulation-optimization performed on future time periods.

References

Bergström S (1976) Development and Application of a Conceptual Runoff Model for Scandinavian Catchments, A: Bulletin series. Department of Water Resources Engineering, Lund Institute of Technology, University of Lund.

Blaney HF, Criddle WD (1962) Determining Consumptive Use and Irrigation Water Requirements. USDA Technical Bulletin 1275, US Department of Agriculture, Beltsville.

Ceola S, Arheimer B, Baratti E, Blöschl G, Capell R, Castellarin A, Freer J, Han D, Hrachowitz M, Hundecha Y, Hutton C, Lindström G, Montanari A, Nijzink R, Parajka J, Toth E, Viglione A, Wagener T (2015) Virtual laboratories: new opportunities for collaborative water science. Hydrol Earth Syst Sci 19:2101-2117. https://doi.org/10.5194/hess-19-2101-2015.

Cornes RC, van der Schrier G, van den Besselaar EJM, Jones PD (2018) An Ensemble Version of the E-OBS Temperature and Precipitation Data Sets. J Geophys Res Atmospheres 123:9391-9409. https://doi.org/10.1029/2017JD028200.

Dosio A (2016) Projections of climate change indices of temperature and precipitation from an ensemble of bias-adjusted high-resolution EURO-CORDEX regional climate models: BIAS-ADJUSTED CLIMATE CHANGE INDICES. J Geophys Res Atmospheres 121:5488-5511. https://doi.org/10.1002/2015JD024411.

Gupta HV, Kling H, Yilmaz KK, Martinez GF (2009) Decomposition of the mean squared error and NSE performance criteria: Implications for improving hydrological modelling. J Hydrol 377:80-91. https://doi.org/10.1016/j.jhydrol.2009.08.003.

Lindström G, Johansson B, Persson M, Gardelin M, Bergström S (1997) Development and test of the distributed HBV-96 hydrological model. J Hydrol 201:272-288. https://doi.org/10.1016/S0022-1694(97)00041-3.

Neri M, Parajka J, Toth E (2020) Importance of the informative content in the study area when regionalising rainfall-runoff model parameters: the role of nested catchments and gauging station density. Hydrol Earth Syst Sci 24:5149-5171. https://doi.org/10.5194/hess-24-5149-2020.

Parajka J, Blöschl G, Merz R (2007) Regional calibration of catchment models: Potential for ungauged catchments. Water Resour Res 43:1-16. https://doi.org/10.1029/2006WR005271.

Tolson BA, Shoemaker CA (2007) Dynamically dimensioned search algorithm for computationally efficient watershed model calibration. Water Resour Res 43. https://doi.org/10.1029/2005WR004723.

Viglione A, Parajka J (2018) TUWmodel: Lumped Hydrological Model for Education Purposes.